Treatment of Acute Thromboembolism in Mice Using Heparin-Conjugated Carbon Nanocapsules

Alan C. L. Tang,[†] Ming-Yao Chang,[‡] Zack C. W. Tang,[†] Hui-Jing Li,[†] Gan-Lin Hwang,[§] and Patrick C. H. Hsieh[†,‡,⊥,*]

[†]Institute of Clinical Medicine and [‡]Department of Biomedical Engineering, National Cheng Kung University & Hospital, Tainan 70428, Taiwan, Republic of China, [§]Nano-Powder and Thin Film Technology Center, Industrial Technology Research Institute, Tainan 709, Taiwan, Republic of China, and [⊥]Institute of Biomedical Sciences, Academia Sinica, Taipei 115, Taiwan, Republic of China

ABSTRACT

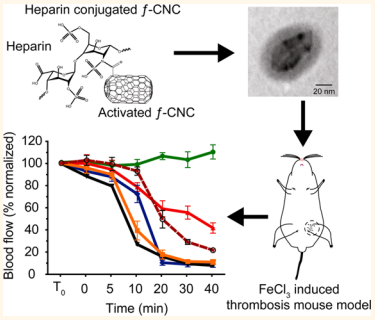

The unsurpassed properties in electrical conductivity, thermal conductivity, strength, and surface area-to-volume ratio allow for many potential applications of carbon nanomaterials in various fields. Recently, studies have characterized the potential of using carbon nanotubes (CNTs) as a biomaterial for biomedical applications and as a drug carrier *via* intravenous injection. However, most studies show that unmodified CNTs possess a high degree of toxicity and cause inflammation, mechanical obstruction from high organ retention, and other biocompatibility issues following *in vivo* delivery. In contrast, carbon nanocapsules (CNCs) have a lower aspect ratio compared with CNTs and have a higher dispersion rate. To investigate the possibility of using CNCs as an alternative to CNTs for drug delivery, heparin-conjugated CNCs (CNC-H) were studied in a mouse model of acute hindlimb thromboembolism. Our results showed that CNC-H not only displayed superior antithrombotic activity *in vitro* and *in vivo* but they also had the ability to extend the thrombus formation time far longer than an injection of heparin or CNCs alone. Therefore, the present study showed for the first time that functionalized CNCs can act as nanocarriers to deliver thrombolytic therapeutics.

KEYWORDS: anticoagulant · drug delivery · heparin · nanoparticle · surface analysis · thrombogenicity

Since the discovery of carbon nanomaterials in the 1960s, billions of dollars have been invested into the development of these nanomaterials for different applications, ranging from optics to structural components.[1,2] For example, the unsurpassed properties of carbon nanotubes (CNTs), including their high mechanical strength, high electrical and thermal conductivity, high surface area-to-volume ratio, and light weight, have made these nanomaterials especially useful in certain biomedical applications.[3−5] The idea of using CNTs as a biomaterial and as a drug carrier has been pursued extensively throughout the past decade. CNTs are ideal for drug delivery because of their high mechanical stability, which allow them to deliver drugs *in vivo* and for a prolonged period. These nanostructured materials also have the versatility to load drugs into the nanotubes as a payload or attached to the surface, as has been previously attempted.[6−9]

However, several properties of CNTs may hinder their use for drug delivery. The van der Waals forces between the surfaces of the CNTs cause aggregation and bundling of the tubes, which prevents homogeneous dispersion. These undesired clumping characteristics of CNTs can induce severe organ disorders, immune responses, and other complications during *in vivo* drug delivery.[10−14] Numerous studies have shown high organ retention and inflammatory effects of CNTs, causing chronic lung inflammation, general granulomatous inflammation, platelet aggregation, and induced or accelerated vascular thrombosis.[15−20] These results indicate the high thrombogenicity of carbon-based nanotubes, which include both single-walled (SWCNTs) and multiwalled CNTs (MWCNTs). Thus, potential risks are involved when carbon-based nanoparticles are used as a biomaterial for *in vivo* drug delivery purposes.[4−6,10−12,21,22] Despite these challenges, CNTs have been modified for higher blood contact compatibility.[23,24] As such, many studies have shown the possibility of using CNTs and graphene-based

* Address correspondence to phsieh@mail.ncku.edu.tw.

Received for review March 19, 2012 and accepted June 19, 2012.

Published online June 19, 2012
10.1021/nn301198r

nanoparticles for drug delivery. Nanoparticles have been visioned as a means to anticoagulant drug delivery for decades.[25] Biomaterials and CNTs have been fabricated and modified to reduce coagulation for drug delivery.[23,26] Heparin, a biological molecule widely used as an anticoagulant, also has been integrated onto CNTs for reducing thrombogenesis.[27]

In addition to the coagulating factor of CNTs, reports have also been published that link the exposure to CNTs with an increased expression of P-selectin and E-selectin, which are key players in the recruitment of leukocytes and their adhesion to the wound site during inflammation.[28,29] Thus, the immunogenic effects of CNTs present some degree of toxicity and may cause side effects in patients if the nanomaterials are used as intravenous drug delivery agents. In recent years, there has been an effort to reduce the toxicity of these carbon-based nanoparticles by surface functionalization.[24] Common tactics have been to employ surface modifications using different polymers to decrease the hydrophobicity of CNTs, thereby augmenting the solubility of the nanomaterials. However, a lack of concrete findings surrounding nanotoxicity and the biocompatibility of CNTs has prevented conclusive agreement on the safety of CNTs for medical use. Thus, comprehensive investigation of *in vivo* toxicity of carbon-based nanomaterials remains to be conducted.[10−12]

In contrast, fullerenes and carbon nanocapsules (CNCs) are very similar carbon-based nanomaterials with several advantages. CNCs are similar to CNTs in that they can be produced by arc discharge and can have shells surrounding a hollow cavity. The overall dimension of CNCs can be kept below 100 nm.[30] Previously, CNCs have been applied in electromagnetic shielding and have found success over CNTs due to a better dispersity in solution and composite matrix.[30,31] Additionally, CNCs have also been utilized in photovoltaic and photocatalytic applications by TiO_2 surface immobilization.[32,33]

Recently, CNCs and nanographene have been modified and tested for drug delivery applications.[34−36] Nanographene has also been shown to provide targeted delivery to tumor sites for imaging purposes.[37,38] PEGylated nanographene also has been achieved to reduce off-target accumulation; nanographene sheets have also been studied for drug delivery and have been touted as an alternative to CNTs.[39,40] In particular, nanographene sheets have high surface area for surface modification and drug conjugation and can be controlled in both dimensions, making it suitable for drug delivery if controlled to nanoparticle dimensions such as CNCs and C_{60}.

These carbon nanomaterials can act as effective drug release agents, as they have been shown to entail less cytotoxicity and thrombogenicity,[41−43] with an advantage of higher surface area-to-volume ratio. Previous studies have identified specific determinants of thrombogenicity by CNTs and have been able to reduce procoagulant tendencies.[23,24,28,43] In contrast, C_{60} fullerene nanoparticles have been observed to not induce or accelerate platelet aggregation when injected intravenously into rats with simultaneous stimulated vascular thrombosis.[28] A number of studies have also concluded that C_{60} has antioxidant effects that inhibit hypersensitivity to allergens in mice.[42,44] In fact, a previous study discovered that repeated delivery of C_{60} fullerene has actually prolonged the lifespan of rats by almost double.[45] Although further studies are required to fully understand the mechanisms involved, the study does illustrate that C_{60} fullerene does not cause any chronic toxicity.

Furthermore, the dispersive rates of these spherical nanoparticles are significantly higher than that of CNTs.[29] Similar to C_{60}, the geometric structure of CNCs is more favorable for drug delivery purposes compared to CNTs. As mentioned previously, CNTs in the raw form aggregate extensively. Postsynthesis cutting of the CNTs must be performed to reduce the overall length of each tube and to reduce the aspect ratio. CNC production does not require this additional step, which results in higher production purity and more even size distributions.[46−48] Although well-studied for its electrical and mechanical properties, CNCs have not been well-established as a biomaterial.[49−51] Recently, we have shown that unmodified CNCs, compared to unmodified CNTs and C_{60}, are highly biocompatible when injected intravenously.[52]

In this study, CNCs were investigated for their potential to act as drug carriers in a mouse model of hindlimb thrombosis. Heparin was chosen for its ability to function as an anticoagulant. We hypothesized that heparin-conjugated CNCs (CNC-H) would increase the local drug concentration, thus enhancing anticoagulant effects while also increasing the half-life of heparin.

RESULTS

Preparation of Heparin-Conjugated Carbon Nanocapsules. Polyhedral hollow CNCs were first fabricated by pulse laser arc discharge. CNCs were then functionalized by sulfuric acid and nitric acid at a ratio of 3:2. This allowed an increase in the dispersion of the capsules and a reduced aggregation *in vivo*. After centrifugation and washing, the CNCs functionalized with carboxyl functional groups were conjugated with heparin *via* 1-ethyl-3-(3-dimethylaminopropyl)carbodiimide (EDC) preactivation (Figure 1A). TEM imaging showed CNCs with an aspect ratio of approximately 1.5 and dimensions of 20−50 nm (Figure 1B). The micrographs of CNC-H also revealed a ring around the CNCs, which is indicative of a layer of heparin encapsulated around the surface of CNCs.

Characterization of Heparin-Conjugated Carbon Nanocapsules. To characterize the CNC-H, samples were lyophilized and analyzed using X-ray photoelectron spectroscopy (XPS). Broad peaks were revealed by the S 2p spectrum

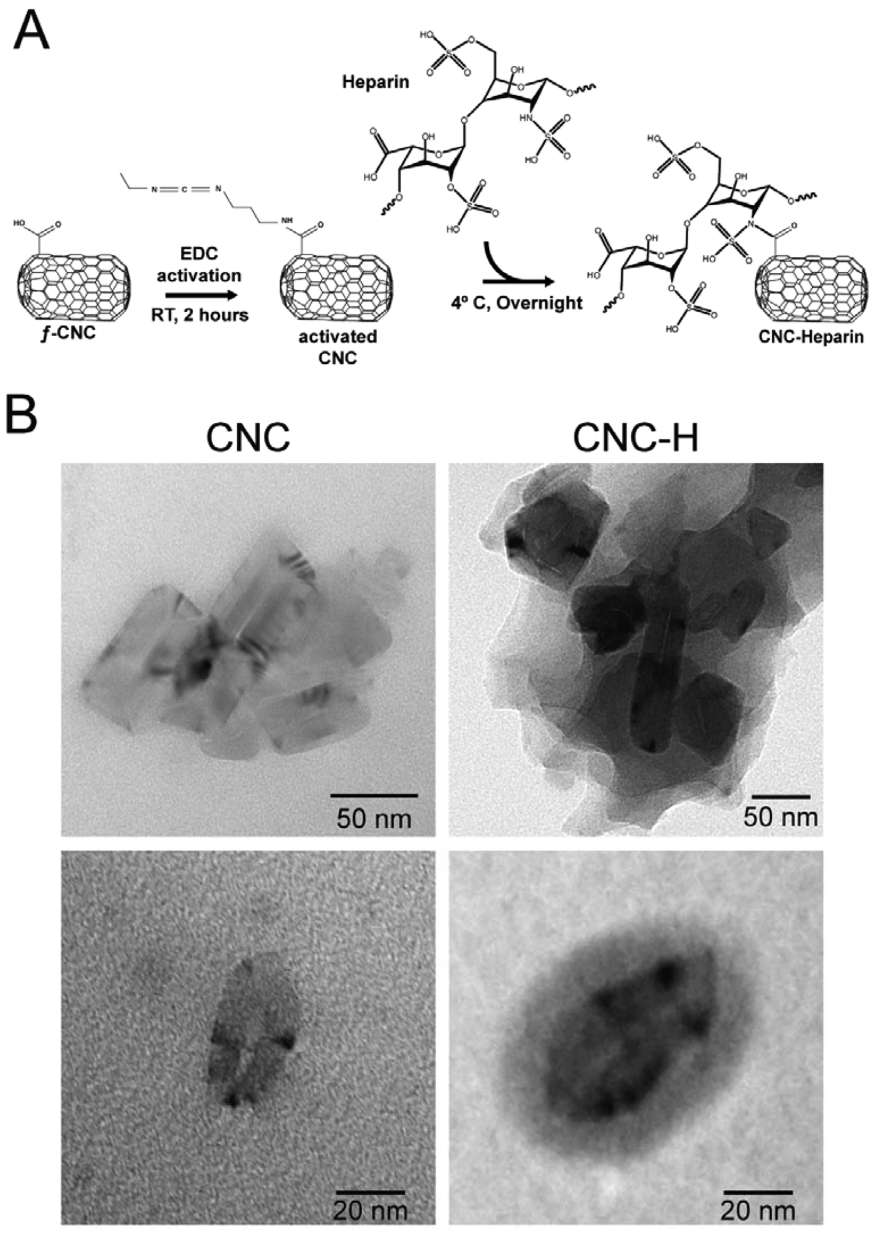

Figure 1. Successful conjugation of heparin onto functionalized carbon nanocapsules. (A) Schematic diagram of heparin conjugation onto functionalized nanocapsules (CNCs) *via* the formation of an amide bond. (B) Transmission electron micrographs of heparin encapsulation around the CNCs.

for both the heparin powder and the CNC-H samples. No peaks were observed for CNC samples in the same S 2p spectrum (Figure 2A). Then, thermogravimetric analysis (TGA) was performed to confirm heparin conjugation by measuring the weight loss of the samples between 200 and 650 °C (Figure 2B). Pure heparin and pure CNC weight loss were first plotted against temperature to serve as a baseline. The heparin-only sample burned between 250 and 650 °C, whereas the CNC powder remained at a temperature beyond 650 °C. The CNC-H powder was then analyzed by plotting the weight *versus* the temperature beyond 650 °C. Anything that burned between 250 and 650 °C was considered to be heparin weight loss. The TGA assay revealed that 37 ± 1.8 wt % of the sample was heparin.

Next, an energy-dispersive X-ray spectroscopy (EDS) analysis of the elements was used to determine the presence of heparin on the surface of heparin-conjugated CNCs by sulfur detection (Figure 3). By performing a reverse calculation using the proportion of sulfur to heparin molecular weight, EDS detected a conjugation efficiency of 30.82 ± 0.06% onto CNCs.

Heparin Activity and Release Profile. In addition to elemental and weight loss analyses, the binding efficiency of heparin onto the functionalized CNCs was determined using the tolonium chloride method.[53] Tolonium chloride reacts with heparin and is used as a colorimetric assay for heparin activity. The supernatants of the CNC-H solutions were extracted and mixed

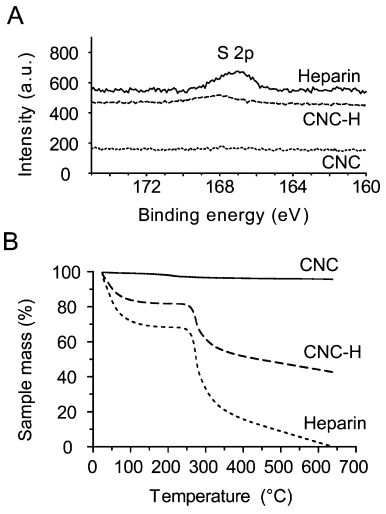

Figure 2. Characterization of heparin-conjugated carbon nanocapsules. (A) X-ray spectroscopy of the S 2p spectrum of heparin, heparin-conjugated carbon nanocapsules (CNC-H), and carbon nanocapsules (CNC). The peak at S 2p reveals the presence of heparin. (B) Thermogravimetric analysis (TGA) of CNC and CNC-H samples. The graph shows 37% mass loss of heparin from CNC-H samples.

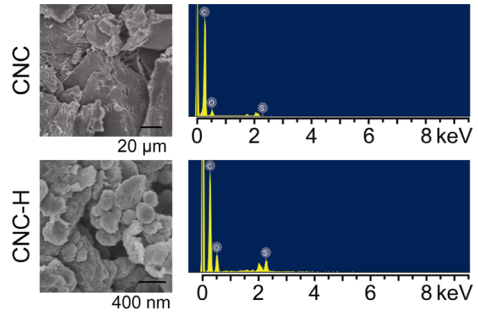

Figure 3. Quantification of heparin conjugation onto functionalized carbon nanocapsules. Energy-dispersive X-ray spectroscopy (EDS) revealed 31% conjugation of heparin onto CNC. Shown are scanning electron micrographs (left panel) and EDS spectra (right panel) of CNC and the CNC-H.

with tolonium chloride and were allowed to react. The samples were detected at 631 nm. A colorimetric assay revealed that the supernatant of the CNC-H solution contained 66.6 ± 2.5% heparin, suggesting that 33.41 ± 2.5% of the heparin was conjugated onto the CNCs (Figure 4A). Additionally, the heparin-conjugated CNCs were left incubated in PBS at 37 °C, and the activity was measured again after 24 h. Heparin activity decreased by roughly 20%, leaving covalently bound heparin on CNC-H at 80% of what was originally detected after conjugation preparation (Figure 4B).

To determine how stable heparin is conjugated onto the CNC-H, samples were incubated in PBS at 37 °C for different time intervals. The samples were then centrifuged, and the supernatants were collected for heparin quantification using a tolonium chloride dye assay similar to that described above. Most of the heparin, assumed to be tangled within each other but not covalently bound to the CNC, was released within 12 h (Figure 4C).

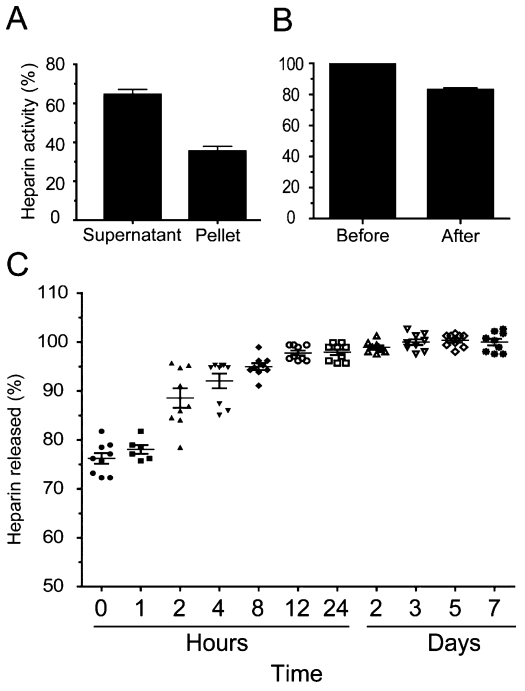

Figure 4. Loading capacity and release profile of heparin-conjugated carbon nanocapsules. The CNC-H heparin conjugation capacity and release profile determined using a tolonium chloride dye reaction. (A) Supernatants from the CNC-H samples were evaluated using a tolonium chloride dye reaction, and heparin conjugation was calculated *via* extrapolation. (B) Heparin activity before and after 24 h incubation in PBS at 37 °C. (C) Release profile of unbound heparin from CNC-H that were incubated in PBS at 37 °C for up to 7 days.

Activated Partial Thromboplastin Time. To determine whether heparin retained its functional activity when conjugated onto the CNCs, an aPTT assay was used to determine the anticoagulant effect of the CNC-H.[54,55] *In vitro* aPTT tests revealed that the CNCs conjugated with heparin effectively prolonged the time until *in vitro* clot formation of blood (Figure 5A). The CNC-H successfully induced the return of aPTT to its normal value, whereas the CNC-only treatment reduced aPTT to less than half of the normal value. Furthermore, *ex vivo* aPTT tests revealed similar results demonstrating the *in vivo* functional ability of the CNC-H treatment (Figure 5B). CNC-H treatment returned the aPTT value to its normal level, whereas the aPTT of the CNC-treated group reduced it to less than half of the normal time. However, the *ex vivo* study showed that simple heparin and the CNC-mixed treatment (CHC/H) increased aPTT significantly beyond the normal physiologic value. To further eliminate any thrombogenic concerns of CNC, we also investigated CNC's ability to activate platelets. Both *in vitro* and *ex vivo* studies showed negative results to CNC activating platelets, compared to adenosine diphosphate (ADP) controls (Supplementary Figure 1).

***In Vivo* Functional Assessment in a Mouse Thromboembolism Model.** To investigate the functional activity of the heparin-conjugated carbon nanocapsules, CNC-H

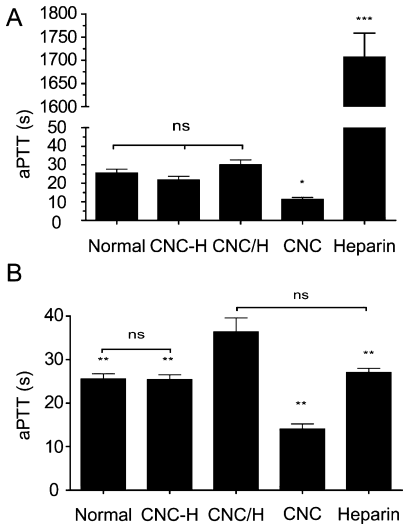

Figure 5. Treatment of heparin-conjugated carbon nanocapsules returns activated thromboplastin times to normal. (A) *In vitro* analysis of the activated thromboplastin time (aPTT) of untreated (normal), CNC-H-treated (CNC-H), CNC and heparin mixed-solution-treated (CNC+H), and CNC-treated (CNC) serum. (B) *Ex vivo* analysis of aPTT of the serum from untreated (normal), CNC-H-injected (CNC-H), CNC+H, and CNC-injected (CNC) mice. *$P < 0.05$, **$P < 0.01$, ***$P < 0.001$ compared with all other groups; ns = not significant.

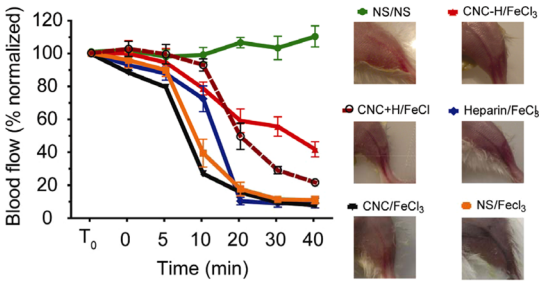

Figure 6. Treatment of heparin-conjugated carbon nanocapsules prevents thrombus formation in a mouse model of acute hindlimb thromboembolism. Mouse hindlimb thromboembolism was induced by ferric chloride. Laser Doppler blood flow measurement of the mice treated with heparin (heparin/$FeCl_3$) or CNCs (CNC/$FeCl_3$) showed significant blood flow decrease, while CNC mixed with heparin (CNC+H) showed gradual decrease of blood flow. In contrast, those treated with CNC-H (CNC-H/$FeCl_3$) showed modest decrease in blood flow compared to untreated normal saline group (NS/$FeCl_3$). The NS/NS group represents normal saline injection into sham mice, and the NS/$FeCl_3$ group represents the thrombosis control treated with ferric chloride. CNC-H-treated group were significantly different than all other groups except CNC+H at the 20, 30, and 40 min time points at $p < 0.01$. CNC-H was significantly different than CNC+H at the 30 and 40 min time points at $p < 0.05$. Also shown are representative photographs of mice hindlimbs 40 min after induced hindlimb thrombosis and treatment.

treatment was intravenously injected into mice after thromboembolism was induced with $FeCl_3$.[56,57] Blood flow monitoring showed that the CNC-H successfully prevented blood flow from falling beneath the cutoff values for the duration of the experiment (Figure 6). Cutoff values were established as the blood flow of the normal saline/$FeCl_3$ (NS/$FeCl_3$)-treated group after 40 min. The CNC mixed with heparin group (CNC+H) also prolonged blood flow decrease but not as well as the CNC-H group. Similarly, heparin-only injections also provided a resistance to a decrease in blood flow up to 10 min after $FeCl_3$ treatment. However, the blood flow abruptly fell below the cutoff value after an additional 5 min. In contrast, the CNC-only treatment decreased the blood flow below 50% in just 10 min after $FeCl_3$ treatment, not significantly different than normal saline injection. Photographs of the diseased limb after 40 min of treatment were taken, which clearly showed oxygen deprivation in the negative treatment control with normal saline for the $FeCl_3$-treated limb.

DISCUSSION

Previous studies using carbon nanomaterials for intravenous drug delivery have had mixed results. Although several groups have shown promising results in various applications, the general consensus on using CNTs for intravenous drug delivery is still relatively reserved.[10−12] Blood contacting applications and systemic delivery of CNTs introduce many issues, such as thrombogenicity, intravenous aggregation, organ retention, and clearance rates, among others.[21,22,28,29,43]

As a solution to the procoagulant activities, CNTs have been surface modified as a mean to diminish the thrombotic effect *in vivo*.[23] System injections of these covalently functionalized MWCNTs are shown to be more biocompatible for drug delivery than pristine MWCNTs. Alternatively, nanographene has also been developed for drug delivery and *in vivo* applications. With high surface area-to-volume ratio and versatility for surface conjugation, nanographene holds similar potential in medicinal applications as CNTs and has seen success in recent studies. However, applying CNTs and nanographene to *in vivo* drug use is still relatively new. Nanoparticle toxicity, particularly carbon-based nanoparticles, is still on its way to being understood at both systemic and tissue levels. These details must be investigated thoroughly to fully characterize the biocompatibility and toxicity of carbon nanomaterials that are used as drug delivery agents for intravenous delivery.

In the present study, alternative carbon-based nanoparticles similar in feature size to nanographene, CNCs, were investigated as potential drug delivery agents. CNCs retain most of the properties of CNTs, including high electroconductivity, thermal conductivity, and strength.[46] Furthermore, functionalized CNCs offer high dispersion rates of up to 40 mg/mL with much lower aspect ratios than most available CNTs. Because the high aspect ratio and aggregating property of unmodified CNTs are the major obstacles to using CNTs for intravenous drug delivery, CNCs offer a suitable advantage in this respect.

To explore the possibility of using CNCs for drug delivery, heparin was conjugated onto functionalized CNCs for intravenous drug delivery in a mouse model of hindlimb thromboembolism. TEM revealed that heparin fully encapsulated the entire carbon nanoparticle. Broad peaks in the XPS S 2p spectrum were exclusively measured in the heparin and CNC-H samples, which showed the presence of sulfur in these two samples but not in the CNC-only samples. To further confirm successful heparin conjugation and to quantify the conjugation, TGA and EDS were used to analyze the CNC-H samples. Consistently, TGA revealed 37 $\pm$ 0.9 wt % of heparin conjugated onto the CNCs. EDS analysis showed the presence of sulfur in the CNC-H samples. Using the sulfur peak area, the amount of heparin weight was reverse calculated, and a 30.8 $\pm$ 0.1 wt % was determined. Therefore, both TGA and EDS detected at least a 30% presence of heparin on the CNC-H samples.

Although the previous assays do definitively demonstrate the presence of heparin on the CNCs after EDC conjugation, the functional activity of the conjugated heparin does not necessarily remain active. To test whether the conjugated heparin retained its biological function, toluidine blue dye was used to assess the heparin activity. A simple colorimetric assay revealed the activity of the heparin in the CNC-H samples and determined a conjugation of 33.4 $\pm$ 2.5%. The aPTT test further confirmed the functional activity of the heparin that was conjugated onto the CNCs. It is worth noting the significant increase in heparin activity above normal levels for the group treated with CNC+H. This elevation in aPTT correlates with known potential risks of using heparin infusion, including the risk of hemorrhage, which prevents large dose injections of heparin. Further platelet activation studies revealed that CNCs do not have any concerns of activating platelets, showing that CNCs are suitable for *in vivo* drug delivery.

Drugs injected intravenously in a bolus have a fast release effect and short half-life, especially heparin. Thus, heparin is usually continuously infused intravenously. The release profile of CNC-H demonstrated a small burst release of noncovalently bound heparin activity. The remaining covalently bound heparin remains conjugated to CNC. However, due to the large surface area-to-volume ratio of the CNC, a higher concentration of heparin is delivered to the thrombus site compared to intravenously injected heparin.

Heparin is an anticoagulant that acts on the extrinsic tissue factor pathway of the coagulation cascade by binding antithrombin or acting as a tissue factor pathway inhibitor.[58−61] Mice treated with $FeCl_3$ patches have been shown to develop acute ischemic disease in several models.[56,57,62] $FeCl_3$ was previously shown to transmigrate through blood vessel walls and to injure endothelial cells by iron exposure.[63,64] As such, denuded blood vessels trigger platelet activation and coagulation and eventually lead to clot formation through the extrinsic pathway because of the exposure of the tissue factor.[65] Therefore, this model is particularly suitable for determining the functional activity of the heparin that was conjugated onto the CNCs.

Laser Doppler blood flow measurements clearly demonstrated the ability of CNC-H to increase the time to thrombus formation and to maintain blood flow for an extended period of time compared with heparin-only injections. Heparin also extended the time to thrombin formation, but at a very limited capacity. When only heparin was injected intravenously, the concentration of heparin significantly decreased immediately upon entering the bloodstream because of the large volume of blood in the circulatory system and the high surface area of all of the tissues and organs. As nanoparticles with a high surface area-to-volume ratio, CNCs effectively concentrate heparin at the surfaces and reduce the dilution of heparin, which permits longer drug activity within the body. The covalent bond between heparin and the carboxyl group effectively prevents release of the heparin, and it is possible that this extended the clearance rate of heparin conjugated onto the CNCs. More studies involving the *in vivo*-conjugated heparin activity will be required to further elucidate the pharmacokinetics of this drug delivery system.

Initial concerns regarding foreign body reactions and thrombus formation after contact with CNC particles do not remain an issue.[21,22] To our surprise, the blood flow pattern of the CNC-only treatment and the normal saline injection did not significantly differ in our mouse hindlimb disease model, contradictory to aPTT results. Potentially, the high blood flow, volume, and circulation eliminated any thrombogenic effects *in vivo*. This indicated that the CNCs did not aggravate additional thrombus formation or any coagulation during the treatment.

The clinical use of heparin for the treatment of thromboembolisms, such as deep vein thrombosis and pulmonary embolism, or for preventing thrombosis after surgery requires a continuous infusion of heparin at high doses.[66] Therefore, it is essential to minimize the innate thrombogenicity of the drugs used while providing a concentrated and targeted drug to the diseased tissue. Future design of this drug delivery system could include targeting molecules to bind to factors elevated by the disease. For example, vWF antibodies could be attached by the biotin−streptavidin conjugation method if the drug is to be delivered after balloon angioplastic surgery where the vessel wall may have been damaged, revealing vWF.

Successful utilization of drug delivery systems could potentially increase the efficacy of drugs, as demonstrated by our system. Accordingly, a smaller amount of drug and a lower frequency of drug administration are achievable, which will provide more convenience

to both patients and health providers. The versatility of functionalized CNCs also enables this drug delivery system to be conjugated with other drugs. Additionally, it is possible to encapsulate a metal inside the CNCs that can be used as a contrast agent to track the nanocapsules, such that the surface is left available for drug loading.[67] Thus, the versatility of CNCs easily transforms nanoparticles into both contrast agents and drug delivery systems that are suitable for intravenous injection.

CONCLUSION

The present study demonstrated the use of CNCs as a heparin drug carrier for the treatment of thrombosis *via* intravenous delivery. Heparin is routinely used for the treatment of deep vein thrombosis and other venous thrombosis diseases. Heparin dosing schemes usually last for weeks to months, and heparin is generally infused intravenously throughout the day. Thus, a controlled drug delivery system is desirable to decrease the initial loading dose and to extend the drug release. Our CNC-H drug carrier conjugated with 30% heparin not only successfully delivered functional heparin *in vivo* but also promoted extended functional anticoagulation effects in a hindlimb thrombosis model. The working time of the heparin was more than doubled when conjugated onto the CNCs. Taken together, we have developed a controlled drug release system using functionalized CNCs that contribute to extended anticoagulation effects of which were demonstrated in our mouse hindlimb acute thrombosis model. Not only can the drug be altered for the treatment of other diseases but the CNCs can also be encapsulated with metals to act as contrast agents. These results provide insight into a novel drug delivery system that provides an alternative to CNTs and that can potentially have applications in a wide range of intravenously delivered drug therapies.

MATERIALS AND METHODS

Multiwalled Carbon Nanocapsule Formulation. CNCs were prepared as described previously.[47,48] Briefly, an inert gas, helium, argon, or nitrogen, was introduced into an arc chamber containing a graphitic cathode and anode. Then, a sufficient voltage (10−30 V) was provided to induce a carbon arc reaction between the cathode and anode. The flowing rate of the inert gas was controlled at approximately 60−90 cm^3/min, and the chamber pressure was 1−2 atm. A pulse current was used (50−70 Hz; 50−500 A), and the deposit on the cathode was collected and passed through a 0.22 μm filter.

Carboxyl Group and Heparin Modification. CNC was dissolved in sulfuric acid/nitric acid (3:2). The solution was stirred at 140 °C and refluxed for 2 h. The carboxyl CNC (CNC-COOH) was then washed with PBS by centrifugation at 18 625*g* until the pH reached 7. The concentration of the carboxyl groups was identified by titration with NaOH at 13 μmol/g CNC. Subsequently, CNC-COOH (0.1 mg/mL) was activated by 1-ethyl-3-(3-dimethylaminopropyl) carbodiimide (EDC, 1 mg/mL, Sigma) for 2 h at room temperature. Sodium heparin (2 IU/mL, Sigma) was added to the previous solution and stirred at 4 °C overnight. The heparin-conjugated CNCs (CNC-H) were lyophilized for characterization.

Transmission Electron Microscopy. The CNC and CNC-H samples were imaged using transmission electron microscopy (TEM, H-7500, Hitachi, Japan) after 10 min of negative staining with phosphotungstic acid (10% w/v; Sigma) and lyophilization overnight.

Thermogravimetric Analysis (TGA). Chambers were purged with nitrogen prior to analysis. Each sample of lyophilized CNC, heparin, or CNC-H was burned in a nitrogen atmosphere of up to 700 °C using a thermogravimetric analyzer (2050, TA Instruments). The sample weight difference between the CNC-H sample and the pure CNC sample in the range of 250 and 700 °C was calculated as heparin. A total of four independent batches of CNC-H were prepared for TGA analysis.

Energy-Dispersive X-ray Spectroscopy (EDS). Lyophilized CNC and CNC-H samples were spread on copper conductive tape (Ted Pella, Inc.) to exclude possible noise from carbon generated by carbon conductive tape. Next, EDS (Axis Ultra DLD, Kratos) was used to identify the elements, such as carbon or sulfur. A total of five independent batches of CNC-H were prepared for EDS analysis.

Tolonium Chloride Dye Reaction. CNC-H was prepared by washing with PBS and centrifuging at 18 625*g* at 4 °C three times. The supernatants were collected separately. Supernatants and 0.005% tolonium chloride dye (Sigma) were mixed together and shaken at a ratio of 1:4 for 3 min. Next, hexane was mixed with the previous solution at a ratio of 1:1 for 3 min. Then, the intensity was detected at 631 nm wavelength.

***In Vitro* Heparin Release Profile.** Fifty micrograms of CNC-H powder was dissolved in 1 mL of PBS and incubated at 37 °C for a series of time points, including 0, 1, 2, 3, 4, 8, 12, 24, 48, 72, 120, and 168 h, and was centrifuged at 18 625*g* and 4 °C. Next, the supernatants were collected for tolonium chloride dye, as described above, to determine the cumulative heparin release activity.

Activated Partial Thromboplastin Time (aPTT). *In vitro* aPTT assays were performed by separating serum from collected wild-type rat blood in citrate and centrifuging at 855*g* and 4 °C for serum collection. Rats were used instead of mice to reduce the numbers of animals used. Treatments (CNC, CNC-H, or heparin), serum, and aPTT test solution (CEPHEN 5, Aniara) were mixed together at a ratio of 1:9:10 and incubated at 37 °C for 3 min. Then, 0.025 μM calcium chloride was added to the samples, and the time was recorded for clot formation. An *ex vivo* study was performed by injecting treatments (2 μg/g w/w) intravenously into the tail vein of rats. After 10 min, whole blood was collected for serum separation, and an aPTT assay was performed by adding calcium chloride to induce clotting. This assay was repeated three times for each group.

Thromboembolism Model. FVB mice 8−12 weeks old and weighing between 20 and 25 g were used for the hindlimb thromboembolism model. Briefly, the mice were anesthetized with Zoteil-50 (50 mg/kg, i.p., Vibrac, France), and the femoral artery and vein of the hindlimb were exposed by piercing through the membranous femoral sheath. The artery and vein were then separated from the nerve for exposure to 5% $FeCl_3$ (Sigma) in a double-distilled H_2O-saturated patch. After 3 min of exposure to 5% $FeCl_3$, the patch was removed, and the incision was sutured with 6-0 sutures. Hindlimb blood flow was measured using laser Doppler flowmetry (O2C flow meter, LEA Medizintechnik, Giessen, Germany).

Animal Model. All animal protocols were approved by the Institutional Animal Care and Use Committee of the National Cheng Kung University. Mice with or without $FeCl_3$-induced thrombosis were injected with normal saline, CNC, CNC-H, or heparin. Injected heparin activity (CHC-H or heparin only) was controlled at 20 U/kg, which was measured using a tolonium chloride dye assay. Normal saline injections with normal saline patches served as the sham/negative control, and normal saline injections with $FeCl_3$ patches served as the positive control. Injections were given through the tail vein immediately after

hindlimbs were introduced to patches. Laser Doppler blood flowmetry was used to measure the blood flow before, during, and after treatments. All blood flow measurements were normalized to the blood flow before the surgery and the treatments. After at least 40 min of blood flow monitoring, photographs of the hindlimbs were taken. There were at least five mice in each group.

Statistical Analysis. All data are presented as the mean ± standard deviation. Statistical analysis was performed using analysis of variance (ANOVA) with a Bonferroni adjustment. A probability value of $P < 0.05$ was considered statistically significant.

Conflict of Interest: The authors declare no competing financial interest.

Acknowledgment. This work was supported by the Taiwan National Science Council (99-3112-B-006-008, 99-2627-M-006-009, 100-2325-B-006-002), the Taiwan National Health Research Institutes (EX-9722SI), the Taiwan Department of Health, Executive Yuan (DOH100-TD-PB-111-TM018), and the Center for Micro/Nano Science and Technology of NCKU (99C028).

Supporting Information Available: Figures, legends, materials and methods for platelet aggregation study. This material is available free of charge *via* the Internet at http://pubs.acs.org.

REFERENCES AND NOTES

1. Baughman, R. H.; Zakhidov, A. A.; de Heer, W. A. Carbon Nanotubes—The Route toward Applications. *Science* **2002**, *297*, 787–792.
2. Li, C.; Chen, Y.; Wang, Y.; Iqbal, Z.; Chhowalla, M.; Mitra, S. A Fullerene-Single Wall Carbon Nanotube Complex for Polymer Bulk Heterojunction Photovoltaic Cells. *J. Mater. Chem.* **2007**, *17*, 2406–2411.
3. Harrison, B. S.; Atala, A. Carbon Nanotube Applications for Tissue Engineering. *Biomaterials* **2007**, *28*, 344–353.
4. Saito, N.; Usui, Y.; Aoki, K.; Narita, N.; Shimizu, M.; Hara, K.; Ogiwara, N.; Nakamura, K.; Ishigaki, N.; Kato, H.; *et al.* Carbon Nanotubes: Biomaterial Applications. *Chem. Soc. Rev.* **2009**, *38*, 1897–1903.
5. Zhang, Y.; Bai, Y.; Yan, B. Functionalized Carbon Nanotubes for Potential Medicinal Applications. *Drug Discovery Today* **2010**, *15*, 428–435.
6. Cheng, W.; Pontoriero, O. T.; Chen, A. M.; He, H. DNA and Carbon Nanotubes as Medicine. *Adv. Drug Delivery Rev.* **2010**, *62*, 633–649.
7. Liu, Z.; Sun, X.; Nakayama-Ratchford, N.; Dai, H. Supramolecular Chemistry on Water-Soluble Carbon Nanotubes for Drug Loading and Delivery. *ACS Nano* **2007**, *1*, 50–56.
8. Podesta, J. E.; Al-Jamal, K. T.; Herrero, M. A.; Tian, B.; Ali-Boucetta, H.; Hegde, V.; Bianco, A.; Prato, M.; Kostarelos, K. Antitumor Activity and Prolonged Survival by Carbon-Nanotube-Mediated Therapeutic siRNA in a Human Lung Xenograft Model. *Small* **2009**, *5*, 1176–1185.
9. Bhirde, A. A.; Patel, V.; Gavard, J.; Zhang, G.; Sousa, A. A.; Masedunskas, A.; Leapman, R. D.; Weigert, R.; Gutkind, J. S.; Rusling, J. F. Targeted Killing of Cancer Cells *in Vivo* and *in Vitro* with Egf-Directed Carbon Nanotube-Based Drug Delivery. *ACS Nano* **2009**, *3*, 307–316.
10. Lacerda, L.; Bianco, A.; Prato, M.; Kostarelos, K. Carbon Nanotubes as Nanomedicines: From Toxicology to Pharmacology. *Adv. Drug Delivery Rev.* **2006**, *58*, 1460–1470.
11. Kostarelos, K. The Long and Short of Carbon Nanotube Toxicity. *Nat. Biotechnol.* **2008**, *26*, 774–776.
12. Kostarelos, K.; Bianco, A.; Prato, M. Promises, Facts, and Challenges for Carbon Nanotubes in Imaging and Therapeutics. *Nat. Nanotechnol.* **2009**, *4*, 627–633.
13. LaVan, D. A.; McGuire, T.; Langer, R. Small-Scale Systems for *In Vivo* Drug Delivery. *Nat. Biotechnol.* **2003**, *21*, 1184–1191.
14. Aillon, K. L.; Xie, Y.; El-Gendy, N.; Berkland, C. J.; Forrest, M. L. Effects of Nanomaterial Physicochemical Properties on *In Vivo* Toxicity. *Adv. Drug Delivery Rev.* **2009**, *61*, 457–466.
15. Baker, G. L.; Gupta, A.; Clark, M. L.; Valenzuela, B. R.; Staska, L. M.; Harbo, S. J.; Pierce, J. T.; Dill, J. A. Inhalation Toxicity and Lung Toxicokinetics of C60 Fullerene Nanoparticles and Microparticles. *Toxicol. Sci.* **2008**, *101*, 122–131.
16. Ryman-Rasmussen, J. P.; Cesta, M. F.; Brody, A. R.; Shipley-Phillips, J. K.; Everitt, J. I.; Tewksbury, E. W.; Moss, O. R.; Wong, B. A.; Dodd, D. E.; Andersen, M. E.; *et al.* Inhaled Carbon Nanotubes Reach the Subpleural Tissue in Mice. *Nat. Nanotechnol.* **2009**, *4*, 747–751.
17. Muller, J.; Huaux, F.; Fonseca, A.; Nagy, J. B.; Moreau, N.; Delos, M.; Raymundo-Piñero, E.; Béguin, F.; Kirsch-Volders, M.; Fenoglio, I.; *et al.* Structural Defects Play a Major Role in the Acute Lung Toxicity of Multiwall Carbon Nanotubes: Toxicological Aspects. *Chem. Res. Toxicol.* **2008**, *21*, 1698–1705.
18. Xu, J. Y.; Li, Q. N.; Li, J. G.; Ran, T. C.; Wu, S. W.; Song, W. M.; Chen, S. L.; Li, W. X. Biodistribution of 99mtc-C60(Oh)Xin Sprague-Dawley Rats after Intratracheal Instillation. *Carbon* **2007**, *45*, 1865–1870.
19. Deng, X.; Jia, G.; Wang, H.; Sun, H.; Wang, X.; Yang, S.; Wang, T.; Liu, Y. Translocation and Fate of Multi-Walled Carbon Nanotubes *in Vivo*. *Carbon* **2007**, *45*, 1419–1424.
20. Poland, C. A.; Duffin, R.; Kinloch, I.; Maynard, A.; Wallace, W. A. A.; Seaton, A.; Stone, V.; Brown, S.; MacNee, W.; Donaldson, K. Carbon Nanotubes Introduced into the Abdominal Cavity Show Asbestos-like Pathogenicity in a Pilot Study. *Nat. Nanotechnol.* **2008**, *3*, 423–428.
21. Dobrovolskaia, M. A.; Germolec, D. R.; Weaver, J. L. Evaluation of Nanoparticle Immunotoxicity. *Nat. Nanotechnol.* **2009**, *4*, 411–414.
22. Dobrovolskaia, M. A.; McNeil, S. E. Immunological Properties of Engineered Nanomaterials. *Nat. Nanotechnol.* **2007**, *2*, 469–478.
23. Murugesan, S.; Park, T. J.; Yang, H.; Mousa, S.; Linhardt, R. J. Blood Compatible Carbon Nanotubes—Nano-based Neoproteoglycans. *Langmuir* **2006**, *22*, 3461–3463.
24. Burke, A. R.; Singh, R. N.; Carroll, D. L.; Owen, J. D.; Kock, N. D.; D'Agostino, R., Jr.; Torti, F. M.; Torti, S. V. Determinants of the Thrombogenic Potential of Multiwalled Carbon Nanotubes. *Biomaterials* **2011**, *32*, 5970–5978.
25. Labhasetwar, V.; Song, C.; Levy, R. J. Nanoparticle Drug Delivery System for Restenosis. *Adv. Drug Delivery Rev.* **1997**, *24*, 63–85.
26. Lassalle, V.; Ferreira, M. L. PLA Nano- and Microparticles for Drug Delivery: An Overview of the Methods of Preparation. *Macromol. Biosci.* **2007**, *7*, 767–783.
27. Park, T. J.; Kim, Y. S.; Hwang, T.; Govindaiah, P.; Choi, S. W.; Kim, E.; Won, K.; Lee, S. H.; Kim, J. H. Preparation and Characterization of Heparinized Multi-walled Carbon Nanotubes. *Process Biochem.* **2012**, *47*, 113–118.
28. Nemmar, A.; Hoet, P. H. M.; Vendervoort, P.; Dinsdale, D.; Nemery, B.; Hoylaerts, M. F. Enhanced Peripheral Thrombogenicity after Lung Inflammation Is Mediated By Platelet-Leukocyte Activation: Role of P-Selectin. *J. Thromb. Haemostasis* **2007**, *5*, 1217–1226.
29. Erdely, A.; Hulderman, T.; Salmen, R.; Liston, A.; Zeidler-Erdely, P.; Schwegler-Berry, D. Cross-Talk between Lung and Systemic Circulation during Carbon Nanotube Respiratory Exposure. Potential Biomarkers. *Nano Lett.* **2009**, *9*, 36–43.
30. Si, P. Z.; Zhang, Z. D.; Geng, D. Y.; You, C. Y.; Zhao, X. G.; Zhang, W. S. Synthesis and Characteristics of Carbon-Coated Iron and Nickel Nanocapsules Produced by Arc Discharge in Ethanol Vapor. *Carbon* **2003**, *41*, 247–251.
31. Cheng, W. H.; Hung, W. C.; Lee, C. H.; Hwang, G. L.; Jou, W. S.; Wu, T. L. Low-Cost and Low-Electromagnetic-Interference Packaging of Optical Transceiver Modules. *J. Lightwave Technol.* **2004**, 22.
32. Huang, H. C.; Huang, G. L.; Chen, H. L.; Lee, Y. D. Immobilization of TiO_2 Nanoparticles on Carbon Nanocapsules for Photovoltaic Applications. *Thin Solid Films* **2006**, *511−512*, 203–207.
33. Huang, H. C.; Huang, G. L.; Chen, H. L.; Lee, Y. D. Immobilization of TiO_2 Nanoparticles on Fe-Filled Carbon Nanocapsules for Photocatalytic Applications. *Thin Solid Films* **2006**, *515*, 1033–1037.
34. Kim, S.; Sergiienko, R.; Shibata, E.; Nakamura, T. Iron-Included Carbon Nanocapsules Coated with Biocompatible Poly(ethylene glycol) Shells. *Mater. Chem. Phys.* **2010**, *122*, 164–168.

35. Kim, S.; Shibata, E.; Sergiienko, R.; Nakamura, T. Purification and Separation of Carbon Nanocapsules as a Magnetic Carrier for Drug Delivery Systems. *Carbon* **2008**, *46*, 1523–1529.
36. Singh, S. K.; Singh, M. K.; Nayak, M. K.; Kumari, S.; Shrivastava, S.; Grácio, J. J.; Dash, D. Thrombus Inducing Property of Atomically Thin Graphene Oxide Sheets. *ACS Nano* **2011**, *5*, 4987–4996.
37. Hong, H.; Zhang, Y.; Engle, J. W.; Nayak, T. R.; Theuer, C. P.; Nickles, R. J.; Barnhart, T. E.; Cai, W. *In Vivo* Targeting and Positron Emission Tomography Imaging of Tumor Vasculature with (66)Ga-Labeled Nano-Graphene. *Biomaterials* **2012**, *33*, 4147–4156.
38. Yang, K.; Zhang, S.; Zhang, G.; Sun, X.; Lee, S. T.; Liu, Z. Graphene in Mice: Ultrahigh *In Vivo* Tumor Uptake and Efficient Photothermal Therapy. *Nano Lett.* **2010**, *10*, 3318–3323.
39. Yang, K.; Wan, J.; Zhang, S.; Zhang, Y.; Lee, S. T.; Liu, Z. *In Vivo* Pharmacokinetics, Long-Term Biodistribution, and Toxicology of PEGylated Graphene in Mice. *ACS Nano* **2011**, *5*, 516–522.
40. Singh, S. K.; Singh, M. K.; Kulkarni, P. P.; Sonkar, V. K.; Grácio, J. J. A.; Dash, D. Amine-Modified Graphene: Thrombo-Protective Safer Alternative to Graphene Oxide for Biomedical Applications. *ACS Nano* **2012**, *6*, 2731–2740.
41. Jia, G.; Wang, H.; Yan, L.; Wang, X.; Pei, R.; Yan, T.; Zhao, Y.; Guo, X. Cytotoxicity of Carbon Nanomaterials: Single-Wall Nanotube, Multi-Wall Nanotube, and Fullerene. *Environ. Sci. Technol.* **2005**, *39*, 1378–1383.
42. Johnston, H. J.; Hutchison, G. R.; Christensen, F. M.; Aschberger, K.; Stone, V. The Biological Mechanisms and Physicochemical Characteristics Responsible for Driving Fullerene Toxicity. *Toxicol. Sci.* **2010**, *114*, 162–182.
43. Radomski, A.; Jurasz, P.; Alonso-Escolano, D.; Drews, M.; Morandi, M.; Malinski, T.; Radomski, M. W. Nanoparticle-Induced Platelet Aggregation and Vascular Thrombosis. *Br. J. Pharmacol.* **2005**, *146*, 882–893.
44. Zolnik, B. S.; González-Fernández, Á.; Sadrieh, N.; Dobrovolskaia, M. A. Minireview: Nanoparticles and the Immune System. *Endocrinology* **2010**, *151*, 458–465.
45. Baati, T.; Bourasset, F.; Gharbi, N.; Njim, L.; Abderrabba, M.; Kerkeni, A.; Szwarc, H.; Moussa, F. The Prolongation of the Lifespan of Rats by Repeated Oral Administration of [60]Fullerene. *Biomaterials* **2012**, *33*, 4936–4946.
46. Su, T. T. Commercialization of Nanotechnology—Taiwan Experiences. IEEE Conference: Emerging Technologies—Nanoelectronics; Meritus Mandarin Hotel, Singapore, **2006**; pp 25—28.
47. Hwang, G. L. Preparation of Hallow Carbon Nanocapsules. U.S. Patent 7156958.
48. Hwang, G. L.; Hwang, K. C.; Shieh, Y. T.; Lin, S. J. Preparation of Carbon Nanotube Encapsulated Copper Nanowires and Their Use as a Reinforcement for Y-Ba-Cu-O Superconductors. *Chem. Mater.* **2003**, *15*, 1353–1357.
49. Chu, C. C.; Hwang, G. L.; Chiou, J. W.; Pong, W. F.; Lin, C. L.; Tsai, C. Y.; Lin, H. M.; Chang, Y. C.; Chang, C. S.; Hsu, A. H.; *et al.* Polymerization of a Confined π-System: Chemical Synthesis of Tetrahedral Amorphous Carbon Nanoballs from Graphitic Carbon Nanocapsules. *Adv. Mater.* **2005**, *17*, 2707–2710.
50. Wang, C.; Huang, C. L.; Chen, Y. C.; Hwang, G. L.; Tsai, S. J. Carbon Nanocapsules-Reinforced Syndiotactic Polystyrene Nanocomposites: Crystallization and Morphological Features. *Polymer* **2008**, *49*, 5564–5574.
51. Su, F. K.; Hong, J. L.; Liao, G. F.; Lin, L. L.; Hwang, G. L.; Day, T. C. Photoluminescent Carbon Nanocapsule/Polycyanate Composites with Hydrogen Bond Interactions. *J. Appl. Polym.* **2006**, *100*, 3784–3788.
52. Tang, A. C.; Hwang, G. L.; Tsai, S. J.; Chang, M. Y.; Tang, Z. C.; Tsai, M. D.; Luo, C. Y.; Hoffman, A. S.; Hsieh, P. C. Biosafety of Non-surface Modified Carbon Nanocapsules as a Potential Alternative to Carbon Nanotubes for Drug Delivery Purposes. *PLoS ONE* **2012**, 7.
53. Jeon, O.; Song, S. J.; Kang, S. W.; Putnam, A. J.; Kim, B. S. Enhancement of Ectopic Bone Formation by Bone Morphogenetic Protein-2 Released from a Heparin-Conjugated Poly(L-lactic-*co*-glycolic acid) Scaffold. *Biomaterials* **2007**, *28*, 2763–2871.
54. Matsubara, S.; Usui, R.; Ohkuchi, A.; Okuno, S.; Izumi, A.; Watanabe, T.; Seo, N.; Suzuki, M. Prolonged Activated Partial Thromboplastin Time in Thromboprophylaxis with Unfractionated Heparin in Patients Undergoing Cesarean Section. *J. Obstet. Gynaecol. Res.* **2010**, *36*, 58–63.
55. Chan, A. K.; Black, L.; Ing, C.; Brandão, L. R.; Williams, S. Utility of aPTT in Monitoring Unfractionated Heparin in Children. *Thromb. Res.* **2008**, *122*, 135–136.
56. Wang, X.; Xu, L. An Optimized Murine Model of Ferric Chloride-Induced Arterial Thrombosis for Thrombosis Research. *Thromb. Res.* **2005**, *115*, 95–100.
57. Owens, A. P., III; Lu, Y.; Whinna, H. C.; Gachet, C.; Fay, W. P.; Machman, N. Towards a Standardization of the Murine Ferric Chloride Carotid Arterial Thrombosis Model. *J. Thromb. Haemost.* **2011**, *9*, 1862–1863.
58. Chuang, Y. J.; Swanson, R.; Raja, S. M.; Olson, S. T. Heparin Enhances the Specificity of Antithrombin for Thrombin and Factor Xa Independent of the Reactive Center Loop Sequence. Evidence for an Exosite Determinant of Factor Xa Specificity in Heparin-Activated Antithrombin. *J. Biol. Chem.* **2001**, *276*, 14961–14971.
59. Crawley, J. T.; Lane, D. A. The Haemostatic Role of Tissue Factor Pathway Inhibitor. *Arterioscler. Thromb. Vasc. Biol.* **2008**, *28*, 233–242.
60. Konstantinides, S.; Schafer, K.; Thinnes, T.; Loskutoff, D. J. Plasminogen Activator Inhibitor-1 and Its Cofactor Vitronectin Stabilize Arterial Thrombi after Vascular Injury in Mice. *Circulation* **2001**, *103*, 576–583.
61. Zhu, Y.; Carmeliet, P.; Fay, W. P. Plasminogen Activator Inhibitor-1 Is a Major Determinant of Arterial Thrombolysis Resistance. *Circulation* **1999**, *99*, 3050–3055.
62. Tseng, M. T.; Dozier, A.; Haribabu, B.; Graham, U. M. Transendothelial Migration of Ferric Ion in $FeCl_3$ Injured Murine Common Carotid Artery. *Thromb. Res.* **2006**, *118*, 275–280.
63. Owens, A. P., III; Lu, Y.; Whinna, H. C.; Gachet, C.; Fay, W. P.; Machman, N. Towards a Stabilization of the Murine Ferric Chloride Carotid Arterial Thrombosis Model. *J. Thromb. Haemost.* **2011**, *9*, 1862–1863.
64. Wu, K. K. Platelet Activation Mechanisms and Markers in Arterial Thrombosis. *J. Intern. Med.* **1996**, *239*, 17–34.
65. Wang, L.; Miller, C.; Swarthout, R. F.; Rao, M.; Mackman, N.; Taubman, M. B. Vascular Smooth Muscle-Derived Tissue Factor Is Critical for Arterial Thrombosis after Ferric Chloride-Induced Injury. *Blood* **2009**, *113*, 705–713.
66. Hirsh, J.; Anand, S. S.; Halperin, J. L.; Fuster, V. Mechanism of Action and Pharmacology of Unfractionated Heparin. Arterioscler. *Thromb. Vasc. Biol.* **2001**, *21*, 1094–1096.
67. Huang, H. C.; Hwang, G. L.; Chen, H. L.; Lee, Y. D. Immobilization of TiO_2 Nanoparticles on Fe-Filled Carbon Nanocapsules for Photocatalytic Applications. *Thin Solid Films* **2006**, *515*, 1033–1037.